Linear-to-Circular Polarization Conversion Using Metasurface

H. L. Zhu, S. W. Cheung, *Senior Member, IEEE*, Kwok Lun Chung, *Senior Member, IEEE*, and T. I. Yuk, *Member, IEEE*

***Abstract*—A metasurface (MS) used to convert the linearly polarized (LP) signal from a source antenna into a circularly polarized (CP) signal is proposed and studied. The MS consists of 16 unit cells arranged in a 4×4 layout. Each unit cell is a rectangular loop with a diagonal microstrip. By placing close to a source antenna, the MS converts the LP signal generated from the source antenna into a CP signal. Two source antennas (patch and slot antennas) are used for studies. The source antenna together with the MS is here called a MS antenna. A total of four low-profile MS antennas operating at the frequency of about 2.45 GHz are designed using computer simulation. For verification of simulation results, the MS antennas are fabricated and measured. Simulated and measured results show good agreements. Results show that the MS antennas have substantially better performances, in terms of gain, return-loss bandwidth (RLBW), axial-ratio bandwidth (ARBW) and radiation pattern, than the source antennas. Moreover, the ARBW of the MS antennas is mainly determined by the MS.**

***Index Terms*—Axial-ratio bandwidth (ARBW), metasurface, metasurfaced antenna, polarizer, return-loss bandwidth (RLBW).**

I. Introduction

METASURFACE (MS), a two-dimensional equivalent of metamaterial, has been attracting attention for researchers [1]–[3]. Some researchers have considered MS as a particular case of frequency-selective surface (such as split-ring resonators, complementary split-ring resonators [4], [5], thin wire media [6] and isotropic elements [7]), which has been well-known for the past 50 years. However, other researchers have considered MS as a new periodic structure different from frequency-selective surface [2]. Many studies have been carried out on using MSs in different applications [1]–[3] and in well-known applications such as compact cavity resonators [8]–[10] and controllable smart surfaces [11]–[13]. Planar antennas have many advantages such as low profile and low cost, but one of the main disadvantages is low gain. The typical directivity of a patch antenna is only about 6 dB and the return-loss bandwidth (RLBW) is proportional to the ratio of the dielectric-slab thickness to the operating wavelength in free space [14]. In general, the thickness of the dielectric-slab is much smaller than the wavelength in free space, so the RLBW of a patch antenna is very narrow (0.5%–3%). These factors restrict the uses of patch antennas to low-gain and narrowband communication systems. MS has a planar structure and can be easily combined with a planar antenna to form new applications, yet maintaining the advantage of low profile and low cost. In [15]–[17], it was proposed to use MS to enhance the RLBW and gain of planar antennas (which are called the source antennas in such applications), yet achieving the low profile characteristic.

In this paper, we propose to use MS to convert the linearly polarized (LP) signal generated from a source antenna into a circularly polarized (CP) signal with wider RLBW and higher gain. In our proposed configuration, the source antenna is placed at a short distance of $1/17\lambda_0$ (where λ_0 is the operating wavelength in free space) from a MS which consists of 16 identical unit cells on a substrate having a size of $\lambda_0 \times \lambda_0$. The same unit cell was used to enhance the performance of a CP patch antenna in [15] which inspired us to use here to convert a LP source antenna into a CP antenna. The main advantages of our proposed design are 1) compact size, 2) simple configuration to achieve LP-to-CP conversion, 3) low cost, 4) using a simple source antenna (patch or slot antenna), and 5) wide operating bandwidth. The basic idea of the MS proposed here was briefly introduced in [18]. As a progress and much more detailed study compared to [18], two simple source antennas, a patch antenna and a slot antenna, together with two MSs having mirror images of each other, are used for detailed investigation in this paper. Results show that the MS can convert a LP signal into a left-handed circularly polarized (LHCP) or right-handed circularly polarized (RHCP) signals at microwave frequencies with excellent performances in terms of the RLBW, axial-ratio bandwidth (ARBW) and realized gain.

To the best knowledge of the authors, there is no other antenna of this kind using the similar approach to convert a LP signal into a CP signal. The one relatively close our approach was presented in [19] which employed a CP reflect array to convert a LP signal generated from a Vivaldi antenna (the source antenna) into a CP signal. The reflect array consisted of 37 unit cells with different sizes in 3 layers and was placed at a distance of about $28\lambda_0$ away. The design had a much larger volume and higher profile than our proposed designs.

II. Design of MS Antennas

The MS antenna proposed here is composed of a MS and a source antenna, both designed using planar technology. The source antenna generates a LP signal which is converted into a CP signal through the use of the MS. Fig. 1(a) shows the

Manuscript received September 21, 2012; revised April 12, 2013; accepted June 03, 2013. Date of publication June 11, 2013; date of current version August 30, 2013.

The authors are with the Department of Electrical and Electronic Engineering, The University of Hong Kong, Hong Kong (e-mail: zhuhl@eee.hku.hk; swcheung@eee.hku.hk; tiyuk@eee.hku.hk).

Color versions of one or more of the figures in this paper are available online at http://ieeexplore.ieee.org.

Digital Object Identifier 10.1109/TAP.2013.2267712

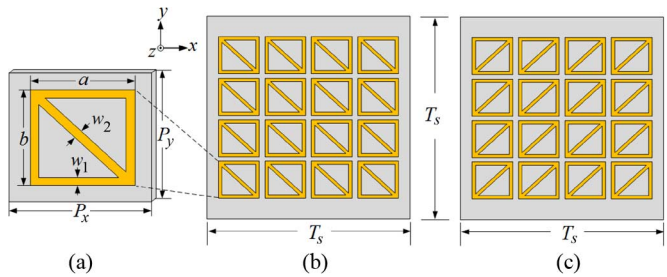

Fig. 1. (a) Unit cell, (b) RH-MS, and (c) LH-MS.

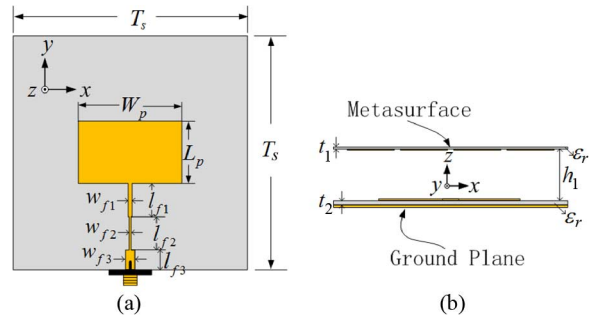

Fig. 2. (a) LP patch antenna (source antenna) and (b) side view of MS antenna.

geometry of the unit cell used in our MSs. Each unit cell is a rectangular loop with a diagonal microstrip. The MSs consist of 16 unit cells in a 4 × 4 arrangement as shown in Fig. 1(b) and (c). The right-handed metasurface (RH-MS) shown in Fig. 1(b) is used to convert a LP signal into a RHCP signal, while the left-handed metasurface (LH-MS) shown in Fig. 1(c), having a mirror image of the RH-MS, is used to convert a LP signal into a LHCP signal.

Two source antennas, a simple patch antenna and a simple slot antenna, are used in our studies to design our MS antennas. Fig. 2 shows one of our proposed MS antennas using a simple patch antenna as the source antenna to generate LP signal for conversion. The patch antenna with microstrip-fed, as shown in Fig. 2(a), has a rectangular patch with a size of $W_p \times L_p = 53 \times 32$ mm^2 printed at the centre of the substrate on one side and a ground on the other side. The microstrip feed line has a two-stage $\lambda/4$-impedance convertors for better impedance matching in the presence of the MS. The MS and patch antenna, as shown in Fig. 2, are designed on two Rogers substrates, RO4350B, having the thicknesses of $t_1 = 0.762$ mm and $t_2 = 1.524$ mm, respectively, with a dielectric constant of $\varepsilon_r = 3.48$ and a lost tangent of $\delta = 0.0031$. They are separated by a cavity height of $h_1 = 6$ mm and, for convenience in implementation, are designed to have the same area of $T_s \times T_s = 120 \times 120$ mm^2. Results have shown that, when the LH-MS shown in Fig. 1(c) is used as the MS in Fig. 2(b), the MS antenna will convert the LP signal generated from the patch antenna into a LHCP signal. This MS antenna is denoted here as MS Ant 1. However, if the LH-MS shown in Fig. 1(b) is used instead, the MS antenna will convert the LP signal into a RHCP signal and the MS antenna is denoted here as MS Ant 2. Since MS Ant 1 is identical to MS Ant 2, except that the MSs used are mirror images of each other, it is expected that they will have the same performance in terms of RLBW, ARBW and realized gain, but orthogonal polarizations. These will be verified by simulation and measurement described later.

Another source antenna used in our studies is a slot antenna having a slot of $L_s \times W_s$ etched at the centre on one side (the ground plane) of the substrate as shown in Fig. 3(a). A 50-Ω feed line is printed on the other side of the substrate. The length L_f and width W_f of the feed line are used for impedance matching. The MS and slot antenna are separated by a cavity height of $h_2 = 7$ mm and, again, for convenience, both the MS and slot antenna are designed to have the same area of 120 × 120 mm^2 and on the Rogers substrates, RO4350B, having the electrical parameters described previously. Simulation results have shown

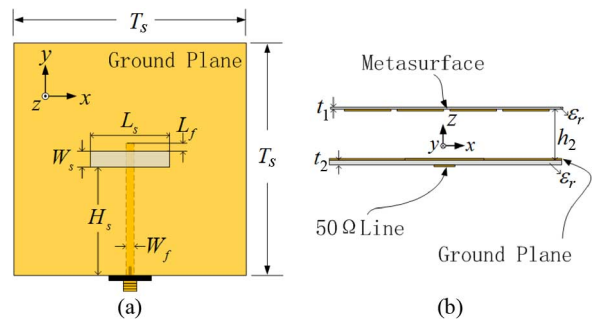

Fig. 3. (a) LP slot antenna (source antenna) and (b) side view of MS antenna.

TABLE I
DIMENSIONS OF MS (UNIT: mm)

P_x	P_y	a	b	w_1	w_2	T_s
26.25	24.15	23.1	22.05	1.05	1.26	120

that using the RH-MS and LH-MS shown in Fig. 1(b) and (c) as the MS in Fig. 3(b) will generate a RHCP and a LHCP signals, respectively, and the corresponding MS antennas are denoted here as MS Ants 3 and 4.

Simulation studies have showed that the four MS antennas can generate CP signals. More studies have showed that, with the use of the MSs, the four MS antennas always have two lowest dips in axial ratio (AR) at around 2.4 and 2.6 GHz, regardless of which source antenna is used. Moreover, the return-loss bandwidths (RLBWs) for RL > 10 dB are much wider than the axial-ratio bandwidths (ARBWs) for AR < 3 dB which therefore determine the operating bandwidths of the antennas. Since the main function of our MS antennas is to convert LP signals into CP signals, the performances of these antennas have been optimized in terms maximizing the ARBW using various parameters of the MS through computer simulation. In the optimization process, we maximized the spacing between the two dips, yet keeping the AR below 3 dB between them. The optimized dimensions of the MS, and the dimensions of the patch antenna and slot antenna are listed in Tables I–III, respectively, which are used to fabricate the MSs, patch antenna and slot antenna as shown in Figs. 4 and 5.

III. STUDY OF METASURFACE

From the optimization process, it is found that the parameters P_x, P_y, a, b and w_1 are most sensitive to the two lowest

TABLE II
DIMENSIONS OF PATCH ANTENNA (UNIT: mm)

W_p	L_p	w_{f1}	w_{f2}	w_{f3}	l_{f1}	l_{f2}	l_{f3}
53	32	2	1	4.8	17	17	10

TABLE III
DIMENSIONS OF SLOT ANTENNA (UNIT: mm)

W_s	L_s	L_f	W_f	H_s
5.8	34	2.5	3	57.1

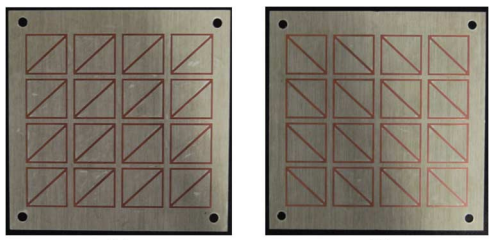

(a) (b)

Fig. 4. (a) LHCP metasurface (LH-MS) and (b) RHCP metasurface (RH-MS).

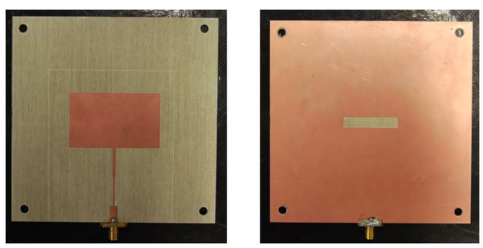

(a) (b)

Fig. 5. (a) Microstrip-fed patch antenna and (b) line-fed slot antenna.

ARs (dips) at around 2.4 and 2.6 GHz, regardless which source antenna is used. Thus a parametric study is carried out on the effects of these parameters on the AR using MS Ant 3 and results are shown in Fig. 6(a)–(e). In these figures, the blue lines show the optimized performance using $P_x = 26.25$, $P_y = 24.15$, $a = 23.1$, $b = 22.05$ and $w_1 = 1.05$ mm in the MS. It can be seen that the AR has two lowest dips of 1 and 0 dB at 2.42 and 2.58 GHz, respectively, and a peak of 2.8 dB at 2.52 GHz between the two dips.

Fig. 6(a) shows that, when P_x is decreased from 26.25 to 25.75 mm, the two dips move away from each other to 2.32 and 2.6 GHz with $\mathrm{AR} = 1$ and 2.5 dB, respectively, but the peak shoots up to 7 dB at 2.5 GHz between the two dips. When P_x is increased to 26.75 mm, the two dips merge together with a minimum AR of 1 dB at 2.54 GHz. Thus P_x can be used to adjust the ARBW. When P_y is increased from 24.15 to 24.65 mm, Fig. 6(b) shows that again the two dips move away from each other with $\mathrm{AR} = 0$ and 0.2 dB at 2.4 and 2.66 GHz, respectively, and the peak shoots up to 7 dB at 2.56 GHz. When P_y is decreased to 23.65 mm, the two dips move towards each other, but the peak shoots up to 13 dB at 2.55 GHz. So P_y has the similar effect to P_x on the ARBW, but in an opposite way. When a is increased from 23.1 to 23.5 mm, Fig. 6(c) shows that only

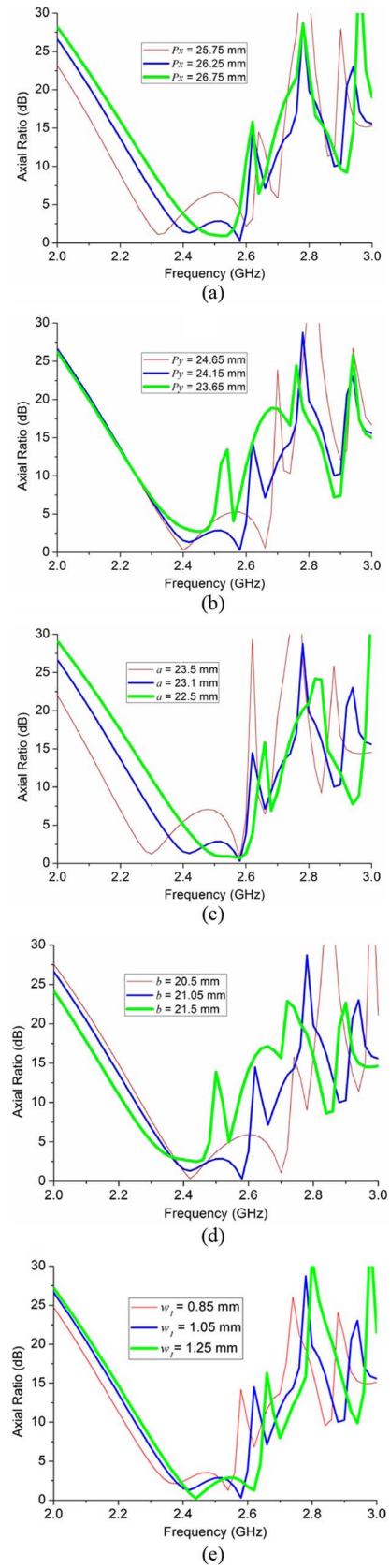

Fig. 6. Simulated AR with different (a) P_x, (b) P_y, (c) a, (d) b, *and* (e) w_1.

the lower-frequency dip shifts down to 2.3 GHz. The higher-frequency dip remains unchanged at 2.58 GHz with $\mathrm{AR} = 0$ dB,

and the peak shoots up to 7 dB at 2.5 GHz. When a is decreased to 22.5 mm, the two dips merge together with a minimum AR of 1 dB at around 2.6 GHz. Thus a can also be used to adjust the ARBW by using the lower-frequency dip. Fig. 6(d) shows that the parameter b affects the higher-frequency dip. When b is decreased from 21.05 to 20.5 mm, the AR of the lower-frequency dip decreases to 0.1 dB with frequency remaining at around 2.42 GHz and the higher-frequency dip shifts up to 2.7 GHz with $\mathrm{AR} = 1$ dB. The peak goes slightly higher to 5 dB at 2.6 GHz. When b is increased from 21.05 to 21.5 mm, the higher-frequency dip shifts down to 2.55 GHz, but the peak shoots up to 14 dB at 2.5 GHz. So b can be used to adjust the ARBW by moving the higher-frequency dip. Fig. 6(e) shows that w_1 affects both the higher- and lower-frequency dips. When w_1 is decreased from 1.05 to 0.85 mm, both higher- and lower-frequency dips shift down to about 2.38 and 2.55 GHz, respectively. The peak is about 3 dB at 2.48 GHz. When w_1 is increased to from 1.05 to 1.25 mm, the two dips shift up to 2.42 and 2.63 GHz. In these two cases, the peak is about the same at 2.8 dB, so w_1 can also be used to adjust the frequencies of both dips.

The E-field distribution has been used to further study the operation of the antenna. The simulated E-field distribution on the MS in the opposite side of the source antenna at 2.4 GHz is shown in Fig. 7, where it is assumed that the phase at which the vertical E-field reaches the maximum is 0°. It can be seen that strong E-fields are emitted from the gaps between the unit cells. At 0° and 180°, the E-fields are mainly emitted from the horizontal gaps, producing vertically LP signals. While at 90° and 270°, the E-fields are mainly emitted from the vertical gaps between the unit cells, producing horizontally LP signals. Thus the vertical and horizontal gaps between the unit cells on the MS take turn to emit a horizontally and vertically LP signals, respectively, generating a CP signal. We have also carried out the same study using the MS without having the diagonal microstrips on the unit cells. Results showed that only the vertical gaps would emit E-fields and so produce no CP signal.

IV. Equivalent Circuit of Metasurface

Here we use equivalent circuits to explain how the proposed MS structure can convert LP to CP. Consider the LH-MS shown in Fig. 1(c) which is used in our proposed antenna to converts LP to CP. The MS is re-drawn in Fig. 8(a), where the pattern enclosed by the red square can be regarded as a new unit cell of the same MS. For convenience in description, the new unit cell is enlarged and shown in Fig. 8(b) with the strips numbered as $\mathrm{s}_0, \mathrm{s}_1, \ldots$, and s_9. Fig. 8(c) shows the same new unit cell with diagonal strips s_8 and s_9 removed. When the LH-MS in Fig. 8(a) is placed close to a source antenna which generates a LP signal as in our MS antenna, an E-field will be developed along the y-axis direction as shown in Fig. 8(b), which can be resolved into two orthogonal components $\overrightarrow{E}_1$ and $\overrightarrow{E}_2$ as shown in the same figure. If the diagonal strips are removed from the unit cell as shown in Fig. 8(c), the component $\overrightarrow{E}_1$ will see the unit cell as a RLC circuit shown in Fig. 9(a) with impedance given by

$$Z = R + j\left(\omega L - \frac{1}{\omega C}\right) \tag{1}$$

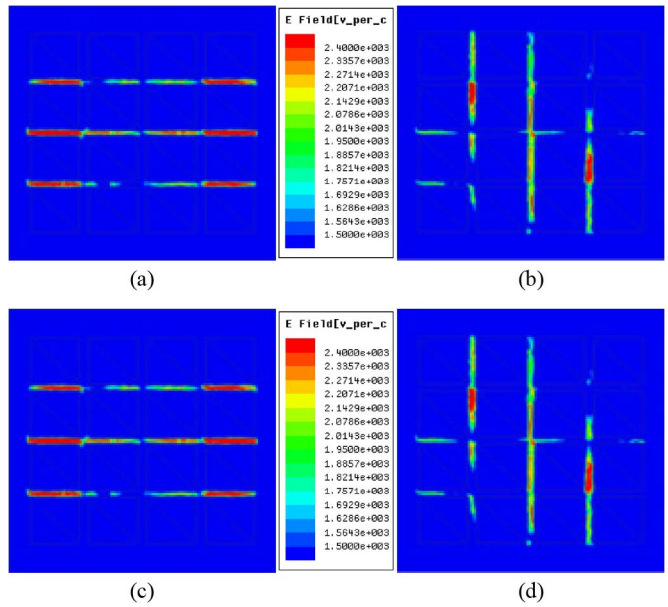

Fig. 7. E-field distribution on MS with diagonal line. (a) 0°; (b) 90°; (c) 180°; (d) 270°.

where C is the capacitance formed by the E-fields across the gaps between strip pairs $(\mathrm{s}_0, \mathrm{s}_1)$, $(\mathrm{s}_2, \mathrm{s}_3)$ and between $(\mathrm{s}_4, \mathrm{s}_5)$ and $(\mathrm{s}_6, \mathrm{s}_7)$, L is the inductance formed by the currents flowing on the strips, and R is the resistance of the strips. For symmetry, the component $\overrightarrow{E}_2$ will also see the same impedance given by (1). If diagonal strips s_8 and s_9 are present in the new unit cell as shown in Fig. 8(b), the impedances Z_1 and Z_2 seen by $\overrightarrow{E}_1$ and $\overrightarrow{E}_2$, respectively, will be changed and different. For $\overrightarrow{E}_1$, the additional E-fields landed on strip s_8 and s_9 will produce capacitance, denoted as C_p here, in parallel with C, with the equivalent shown in Fig. 9(b). The resultant capacitance of $C//C_p$ is less than C and so making Z_1 less capacitive than Z. Whereas for $\overrightarrow{E}_2$, the additional currents flowing on strips s_8 and s_9 will produce inductance, denoted as L_p here, in parallel with L, with the equivalent circuit shown in Fig. 9(c). The resultant inductance of $L//L_p$ is less than L and so making Z_2 less inductive. Since Z_1 is less capacitive than Z and Z_2 is less inductive than Z, $\overrightarrow{E}_1$ will lead $\overrightarrow{E}_2$ by $\mathrm{ang}(Z_1 - Z_2)$ after going through the MS. From Fig. 9(b) and (c), the impedances Z_1 and Z_2 can be written, respectively, as

$$Z_1 = R_1 + j\left(\omega L - \frac{1}{\omega(C//C_p)}\right) \tag{2}$$

$$Z_2 = R_2 + j\left(\omega(L//L_p) - \frac{1}{\omega C}\right). \tag{3}$$

If the MS is designed such that $|Z_1| = |Z_2|$ and $\mathrm{ang}(Z_1 - Z_2) = 90°$, the resultant E-field will be LHCP and rotating in the anticlockwise direction. In the above analysis, if the RH-MS in Fig. 1(b) is used instead, then the diagonal strips will cause Z_1 and Z_2 to be less inductive and less capacitive, respectively, than Z. As a result, $\overrightarrow{E}_1$ will be lagging $\overrightarrow{E}_2$ and the resultant E-field will be RHCP and rotating in the clockwise direction. This analysis agrees with our simulation and measurement.

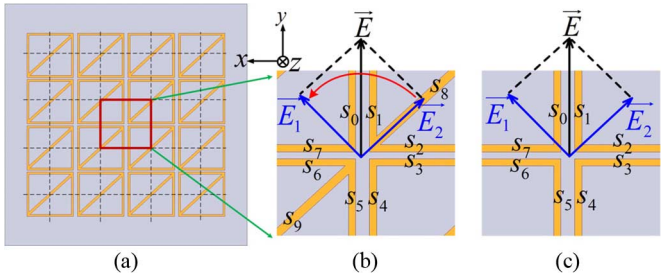

Fig. 8. (a) LH-MS, (b) new unit cell, and (c) new unit cell with diagonal strips removed.

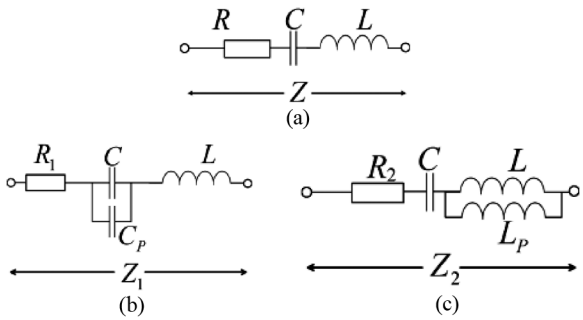

Fig. 9. Equivalent circuits of (a) new unit cell with diagonal strips removed seen by $\vec{E}_1$ and $\vec{E}_2$, (b) new unit cell seen by $\vec{E}_1$, and (c) new unit cell seen by $\vec{E}_2$.

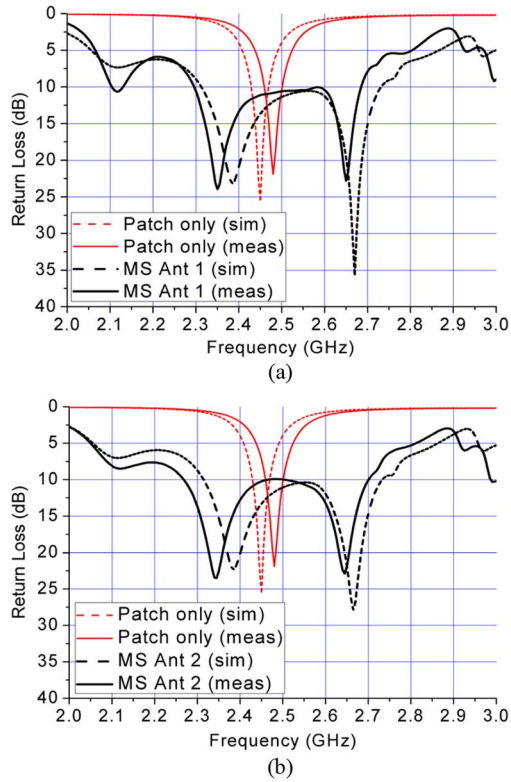

Fig. 10. Simulated and measured RLs of patch antenna only and (a) MS Ant 1 and (b) MS Ant 2.

V. Simulation and Measurement Results

The patch antenna, the slot antenna and the MS antennas have been studied, designed and optimized using computer simulation. For verification of the simulation results, these antennas have been fabricated using our prototype machine and measured using the antenna measurement system, Satimo Starlab.

A. Return-Loss Bandwidth

The simulated and measured return losses (RLs) of the patch antenna, MS Ants 1 and 2, are shown in Fig. 10, and the RLs of the slot antenna, MS Ants 3 and 4 are in Fig. 11. It can be seen that the simulated results agree well with the measured results. The differences are due to 1) the fabrication tolerances of the prototype machine in our laboratory (which could make the narrowest microstrip line of only 0.2 mm), 2) the alignment tolerance of the source antenna with the MS in assembling the MS antenna, and 3) the measurement uncertainty. Fig. 10 shows that, the patch antenna alone has a measured RLBW (for RL $>$ 10 dB) of only about 50 MHz (a fractional bandwidth of only 2%). With the use of the MS, the RLBWs are substantially increased to 380 MHz (a fractional bandwidth of 15.5%), from 2.3 to 2.68 GHz, for MS Ant 1, and to 430 MHz (17.6%), from 2.27 to 2.7 GHz, for MS Ant 2. Note that both MS antennas have similar performances (but different polarizations as shown later) for the reason described previously. For the slot antenna alone, Fig. 11 shows that the measured RLBWs are only about 200 MHz. However, when the MS is used, the RLBWs for MS Ants 3 and 4 are substantially increased to 630 MHz (25.7%), from 2.05 to 2.68 GHz, and to 615 MHz (25.1%), from 2.075 to 2.69 GHz, respectively. Again, both MS antennas have similar performances (but orthogonal polarizations as shown later).

These results show that the RLBWs can be substantially increased by using the MSs. The reason for the improvements of RLBW, in fact, can be seen in the results of Figs. 10 and 11, which indicate that the source antennas have only one resonance in the frequency band from 2 to 3 GHz, but the MS antennas have more than one resonance across the same frequency band. Thus to increase the RLBW, the dimensions of MS antenna should be adjusted to generate more resonances at the appropriate frequencies.

B. Axial-Ratio Bandwidth

In the design of CP antennas, AR is one of the important factors to be considered. The simulated and measured ARs in the boresight of the MS antennas are shown in Fig. 12. The simulated and measured results in general agree well. It can be seen that the higher-frequency dips in the measured results are about 40 MHz lower than those of the simulated results and with reduced deepness. As described previously, the differences are due to 1) the fabrication tolerance, 2) the alignment tolerance, and 3) the measurement uncertainty. It should be noted that the AR is quite sensitive to the dimensions of the MS, as shown in Fig. 6(a)–(e). A small change of 0.5 mm in "P_y," "P_y," or "b" of the unit cells can easily alter the frequency and deepness of the AR dip. Since the smallest dimension that we can fabricate antennas using the prototype-machine in our laboratory is 0.2 mm, the fabrication tolerance could easily cause discrepancies between the simulated and measured results.

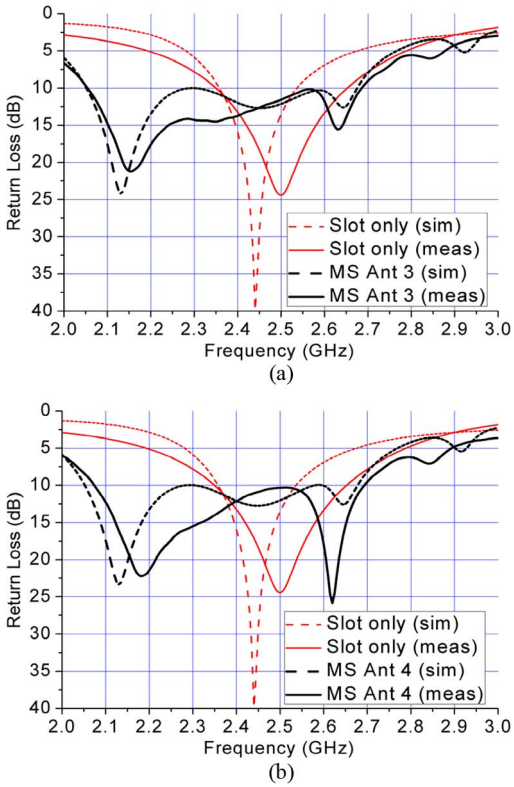

Fig. 11. Simulated and measured RLs of slot antenna only and (a) MS Ant 3 and (b) MS Ant 4.

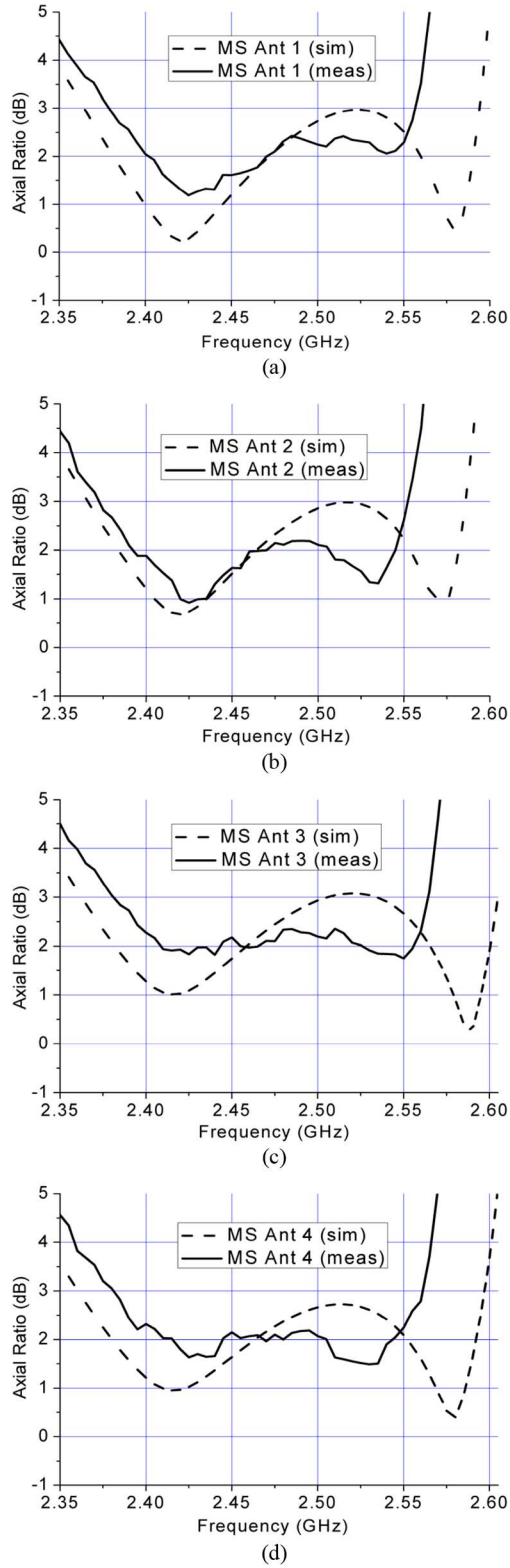

Fig. 12. Simulated and measured ARs of (a) MS Ant 1, (b) MS Ant 2, (c) MS Ant 3, and (d) MS Ant 4.

The results in Fig. 12 indicate that the ARBW is determined by the MS, instead of the source antenna. The ARBWs of the four MS antennas are less than the RLBWs shown in Figs. 10 and 11, and so determine the operating bandwidths of the antennas.

More simulation tests have been carried out to study the frequency response of AR for the CP signal at different angles θ of incidence in the far field. MS Ant 3 has been used for study and results are shown in Fig. 13. It can be seen that the ARBW (for $\mathrm{AR} < 3$ dB) reduces as the angle of incidence in the xz or yz planes deviates from 0°. This is because the MS antennas has been maximized in term of ARBW for $\mathrm{AR} < 3$ dB at the boresight, so any change in the optimized condition will reduce the ARBW. Of course, if the MS antenna is designed to operate at a large angle of incidence, then maximizing θ should be used as the criterion for optimization in the design process.

C. Realized Gain

The simulated and measured results of the realized LHCP and RHCP gains of the MS antennas are shown in Fig. 14. For comparison, the co-polar gains of the LP source antennas are also shown in the same figures. The cross-polar gains of the source antennas are too small to be shown in the same figure and so are omitted. It can be seen that the simulated and measured results have good agreements. Fig. 14(a) shows that the patch antenna alone has a measured 5-dB bandwidth of only 50 MHz (from 2.47 to 2.52 GHz) and a measured peak gain of 5.8 dB at the 2.48 GHz. By adding the LH-MS, MS Ant 1 has the realized LHCP and RHCP gains of about 9 and -12 dB, respectively, at 2.45 GHz. The LH-MS, acting like a polarizer, changes the polarization of the source antenna from LP to LHCP. MS Ant 1 offers a 5-dB enhancement in the realized gain at 2.45 GHz and achieves about 8-dB in the operating bandwidth from 2.38 to 2.56 GHz. Fig. 14(b) shows that MS Ant 2 has the very similar

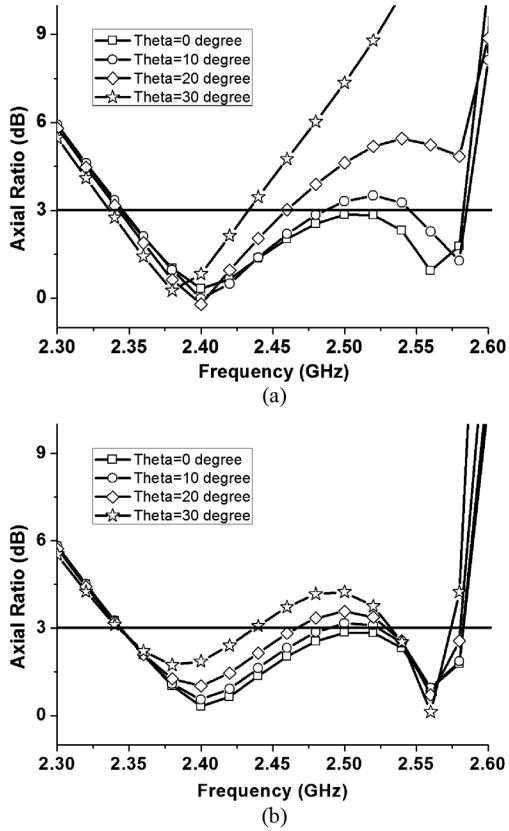

Fig. 13. AR at different incident angles θ in (a) xz-plane and (b) yz-plane.

performances, but orthogonal polarization to that of MS Ant 1 due to the mirror image of the MS used. This result indicates that polarization of the MS antenna is determined by the diagonal microstrips on the unit cells.

For the slot antenna alone, the measured gain at 2.45 GHz is about 3.4 dB. When the LH-MS is used, Fig. 14(c) shows that MS Ant 3 has a LHCP gain of 7.7 dB and a very low RHCP gain of −11 dB at 2.45 GHz. Again, the LH-MS acts as a polarizer to convert the LP signal from the slot antenna into a LHCP signal and, at the same time, enhances the gain by 4.3 dB. When the MS is replaced by a RH-MS, the performance of MS Ant 4 remains similar but with polarization changed to RHCP.

D. Radiation Pattern

The simulated and measured radiation patterns of the source antennas, MS Ants 1, 2, 3 and 4 at 2.45 GHz are shown in Figs. 15 and 16. It can be seen good agreements between the simulated and measured results. Moreover, the radiation patterns for MS Ants 1 and 2 (as shown in Fig. 15) are very similar for the reason previously. This also occurs to MS Ants 3 and 4 (as shown in Fig. 16). Fig. 15 shows that, with using the MSs, the radiation patterns of MS Ants 1 and 2 become more directional toward the z- direction when compared with that of the patch antenna alone. Note that the MS is placed in the z-direction of the source antenna and so the power is more concentrated in the direction toward the MS. Here the MS receives the LP signal from the source antenna and re-radiates the signal in CP to the other side in the opposite direction. The increase in directivity can be seen in the half-power beamwidth (HPBW) and

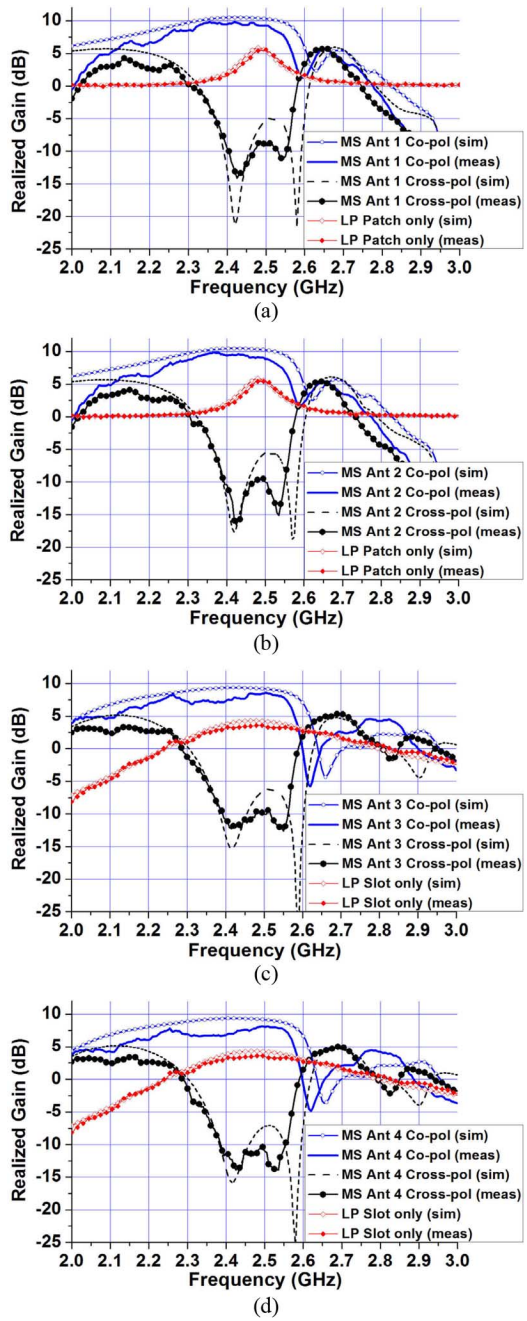

Fig. 14. Simulated and measured realized gains of source antennas and (a) MS Ant 1, (b) MS Ant 3, (c) MS Ant 3 and, (d) MS Ant 4.

front-to-back ratio (FBR) of the radiation pattern. For the patch antenna alone, the measured HPBW in the xz- and yz-planes are both about 74°, as can be seen in Fig. 15. After adding the LH-MS, the HPBW is reduced to about 50° in both the xz- and yz-planes. The measured FBR of the patch antenna is also increased from 16 to 26 dB by using the MS.

For the slot antenna, the increases in directivity using the MSs are particularly obvious, as can be seen in Fig. 16. When no MS is used, the slot antenna has a bi-directional radiation pattern pointing at the positive and negative z-directions, with the measured HPBWs of about 84° and 62° in the xz- and yz-planes, respectively, and the measured FBR of about 0 dB. When the MSs are used, the HPBWs are reduced to about 54° in both the

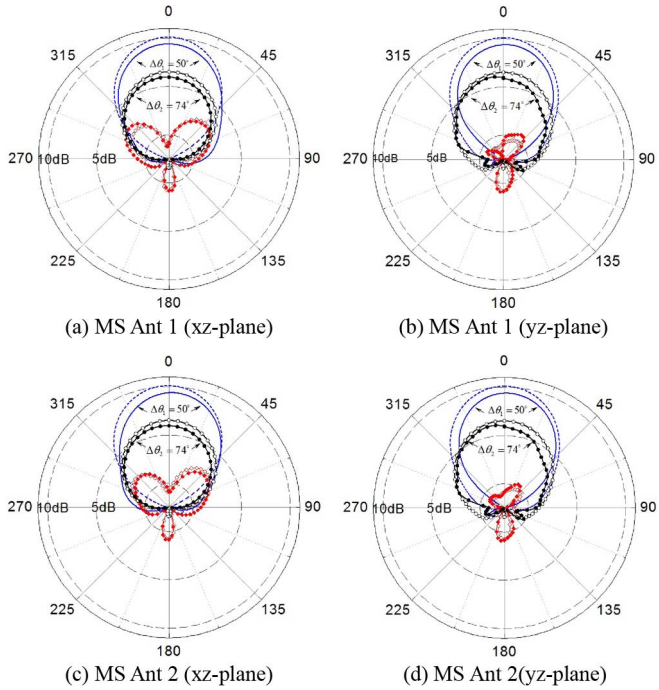

(a) MS Ant 1 (xz-plane) (b) MS Ant 1 (yz-plane)

(c) MS Ant 2 (xz-plane) (d) MS Ant 2(yz-plane)

Fig. 15. Radiation patterns of patch antenna only, with LH-MS at 2.45 GHz in (a) xz-plane and (b) yz-plane, and with RH-MS at 2.45 GHz in (c) xz-plane and (d) yz-plane. (_ _ _: Sim. Co-pol, ——: Mea. Co-pol, —◇—: Sim. Cross-pol, —◆—: Mea. Cross-pol, —○—: Sim. Patch only, —●—: Mea. Patch only.). (a) MS Ant 1 (xz-plane); (b) MS Ant 1 (yz-plane); (c) MS Ant 2 (xz-plane); (d) MS Ant 2 (yz-plane).

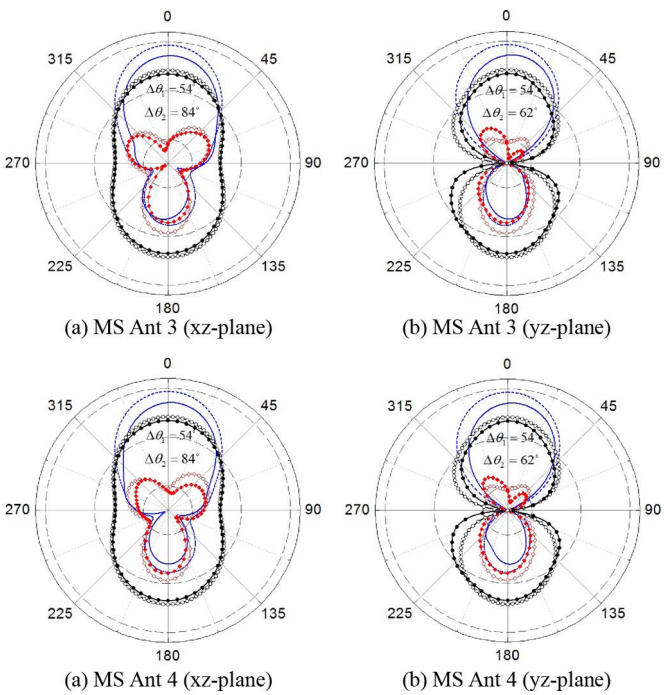

(a) MS Ant 3 (xz-plane) (b) MS Ant 3 (yz-plane)

(a) MS Ant 4 (xz-plane) (b) MS Ant 4 (yz-plane)

Fig. 16. Radiation patterns of slot antenna only, with LH-MS at 2.45 GHz in (a) xz-plane and (b) yz-plane, and with RH-MS at 2.45 GHz in (c) xz-plane and (d) yz-plane. (_ _ _: Sim. Co-pol, ——: Mea. Co-pol, —◇—: Sim. Cross-pol, —◆—: Mea. Cross-pol, —○—: Sim. Slot only, —●—: Mea. Slot only.). (a) MS Ant 3 (xz-plane); (b) MS Ant 3 (yz-plane); (c) MS Ant 4 (xz-plane); (d) MS Ant 4 (yz-plane).

xz- and yz-planes, and the FBR increased to about 11 dB, as shown in Fig. 16.

VI. Conclusion

A MS used for LP-to-CP conversion has been presented in this paper. Two simple antennas, a slot antenna and a patch antenna, are used as source antenna to generate LP signals for conversion. Results have showed that the MS can effectively convert the LP signals from the source antennas into the CP signals, with substantial enhancements in the RLBW, ARBW and realized gain. By using the mirror image of the unit cells on the MS, an orthogonal CP signal is obtained. Thus the MS provides a convenient way to generate CP signals at microwave frequencies.

References

[1] C. L. Holloway, A. Dienstfrey, E. F. Kuester, J. F. O'Hara, A. K. Azad, and A. J. Taylor, "A discussion on the interpretation and characterization of metafilms/metasurfaces: The two-dimensional equivalent of metamaterials," *Metamaterials*, vol. 3, no. 2, pp. 100–112, Oct. 2009.

[2] C. L. Holloway, E. F. Kuester, J. A. Gordon, J. F. O'Hara, J. Booth, and D. R. Smith, "An overview of the theory and applications of metasurfaces: The two-dimensional equivalents of metamaterials," *IEEE Antennas Propag. Mag.*, vol. 54, no. 2, pp. 10–35, Apr. 2012.

[3] C. L. Holloway, D. Love, E. F. Kuester, J. A. Gordon, and D. A. Hill, "Use of generalized sheet transition conditions to model guided waves on metasurfaces/metafilms," *IEEE Trans. Antennas Propag.*, vol. 80, no. 11, pp. 5173–5186, Nov. 2012.

[4] I. Al-Naib, R. Singh, M. Shalaby, T. Ozaki, and R. Morandotti, "Engineering the response of terahertz metasurfaces by spatial arrangement of split-ring resonators," in *Proc. Lasers and Electro-Optics (CLEO) Conf.*, 2012, pp. 1–2.

[5] M. Beruete, R. Marques, J. D. Baena, and M. Sorolla, "Resonance and cross-polarization effects in conventional and complementary split ring resonators periodic screens," in *Proc. IEEE Antennas and Propagation Society Int. Symp.*, 2005, vol. 3A, pp. 794–797.

[6] V. F. Fusco, "Antenna possibilities using 2D planar periodic structures," in *Proc. Int. Workshop Antenna Technology: Small and Smart Antennas Metamaterials and Applications*, 2007, pp. 91–94.

[7] J. D. Baena, L. Jelinek, R. Marques, J. J. Mock, J. Gollub, and D. R. Smith, "Isotropic frequency selective surfaces made of cubic resonators," *App. Phys. Lett.*, vol. 91, no. 19, pp. 191105–191113, 2007.

[8] C. L. Holloway, D. C. Love, E. F. Kuester, A. Salandrino, and N. Engheta, "Sub-wavelength resonators: On the use of metafilms to overcome the lambda/2 size limit," *IET Microw., Antennas, Propag.*, vol. 2, no. 2, pp. 120–129, 2008.

[9] M. Caiazzo, S. Maci, and N. Engheta, "A metamaterial surface for compact cavity resonators," *IEEE Antenna Propag. Lett.*, vol. 3, no. 12, pp. 261–264, Dec. 2004.

[10] S. N. Burokur, R. Yahiaoui, and A. de Lustrac, "Subwavelength resonant cavities fed by microstrip patch array," in *Proc. IEEE Int. Workshop Antenna Technology*, Mar. 2–4, 2009, pp. 1–4.

[11] S. N. Burokur, J. P. Daniel, P. Ratajczak, and A. de Lustrac, "Tunable bilayered metasurface for frequency reconfigurable directive emissions," *Appl. Phys. Lett.*, vol. 97, no. 6, pp. 064101–064101-3, Aug. 2010.

[12] C. L. Holloway, M. A. Mohamed, E. F. Kuester, and A. Dienstfrey, "Reflection and transmission properties of a metafilm: With an application to a controllable surface composed of resonant particles," *IEEE Trans. Electromagn. Compat.*, vol. 47, no. 4, pp. 853–865, Nov. 2005.

[13] G. Minatti, S. Maci, P. De Vita, A. Freni, and M. Sabbadini, "A metasurface isoflux antenna and potential beam reconfigurability," in *Proc. 6th Eur. Conf. Antennas and Propagation (EUCAP)*, Mar. 26–30, 2012, pp. 2613–2617.

[14] J. D. Kraus and R. J. Marhefka, *Antennas For All Applications*, 3rd ed. New York, NY, USA: McGraw-Hill, 2006.

[15] K. L. Chung and S. Chaimool, "Diamagnetic metasurfaces for performance enhancement of microstrip patch antennas," in *Proc. Eur. Conf. Antennas and Propagation (EUCAP)*, 2011, pp. 56–60.

[16] S. Chaimool, C. Rakluea, and P. Akkaraekthalin, "Low-profile unidirectional microstrip-fed slot antenna using metasurface," in *Proc. Int. Symp. Intelligent Signal Processing and Communications Systems (ISPACS)*, Dec. 7–9, 2011, pp. 1–5.

[17] C. Rakluea, S. Chaimool, P. Rakluea, and P. Akkaraekthalin, "Unidirectional CPW-fed slot antenna using metasurface," in *Proc. 8th Int. Conf. Electrical Engineering/Electronics, Computer, Telecommunications and Information Technology (ECTI-CON)*, May 17–19, 2011, pp. 184–187.
[18] H. L. Zhu, K. L. Chung, X. L. Sun, S. W. Cheung, and T. I. Yuk, "CP metasurfaced antennas excited by LP sources," presented at the IEEE Int. Symp. Antennas and Propagation, Chicago, IL, USA, Jul. 2012.
[19] Z. H. Wu, W. X. Zhang, Z. G. Liu, and W. Shen, "Circularly polarised reflectarray with linearly polarised feed," *Electron. Lett.*, vol. 41, Mar. 2005.

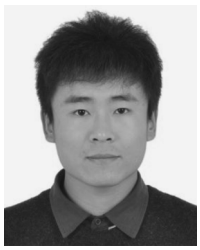

H. L. Zhu received the B.Eng. degree in information engineering and the M.S. degree in electromagnetic field and microwave engineering from the Beijing Institute of Technology, Beijing, China, in 2009 and 2011, respectively. He is currently pursuing the Ph.D. degree in electrical and electronic engineering at the University of Hong Kong, Hong Kong, China.

His research interests include antenna design and study of metasurface.

S. W. Cheung (SM'08) received the B.Sc. degree with First Class Honours in electrical and electronic engineering from Middlesex University, U.K., in 1982, and the Ph.D. degree from Loughborough University of Technology, U.K., in 1986.

From 1982 to 1986, he was a Research Assistant in the Department of Electronic and Electrical Engineering, Loughborough University of Technology, where he collaborated with Rutherford Appleton Laboratory and many U.K. universities to work a project for new generations of satellite systems. He is an Associate Professor at the University of Hong Kong in charge of the Microwave, RF Frequency and Telecom Laboratories. His current research interests include antenna designs, 2G, 3G, and 4G mobile communications systems, MIMO systems, and satellite communications systems.

Dr. Cheung has been serving the IEEE in Hong Kong for the past 20 years. In 2009 and 2010, he was the Chairman of the IEEE Hong Kong Joint Chapter on Circuits and Systems and Communications. He was the Honorary Treasurer and currently the Chair-Elect of the IEEE Hong Kong.

Kwok Lun Chung (S'00–M'05–SM'11) was born in Hong Kong. He received the B.E. degree with first-class honors and the Ph.D. degree in electrical engineering from the University of Technology Sydney (UTS), Australia, in 1999 and 2005, respectively.

He joined the Faculty of Engineering, University of Technology Sydney, in 2004 as a Lecturer. Two years later, he moved to the Department of Electronic and Information Engineering at the Hong Kong Polytechnic University, where he spent about six years. He returned to Sydney, Australia, in 2012, and he is currently working at the Institute for Infrastructure Engineering, University of Western Sydney (UWS) as a Research Fellow for Infrastructure Health Monitoring. His current research interests include wireless sensors for structure health monitoring, microwave antennas, applications of metamaterials and metasurfaces, and wireless power harvesting.

Dr. Chung was the Vice-chair and Chairman of the IEEE AP/MTT Hong Kong Joint Chapter in 2010 and 2011, respectively.

T. I. Yuk (M'86) received the B.S. degree from Iowa State University, Ames, IA, USA, in 1978 and the M.S. and Ph.D. degrees from Arizona State University, Phoenix, AZ, USA, in 1980 and 1986, respectively.

Since 1986, he has been teaching at the University of Hong Kong. His current research interests include wireless communications and antenna designs.